3dSpAn: an interactive software for 3D segmentation and analysis of dendritic spines

Subhadip Basu[1*†], Nirmal Das[1], Ewa Baczynska[2,3], Monika Bijata[2], Andre Zeug[7], Dariusz Plewczynski[4,5], Punam Kumar Saha[6], Evgeni Ponimaskin[7] and Jakub Wlodarczyk[2†]

Abstract

Background: 3D segmentation and analysis of dendritic spines involve two major challenges: 1) how to segment individual spines in 3D from the dendrites and 2) how to quantitatively assess the 3D morphology of individual spines. We developed software named *3dSpAn* to address these two issues by implementing a 3D multiscale opening algorithm in shared intensity space and using effective morphological features, for individual dendritic spine plasticity analysis.

Results: 3dSpAn works in four main modules: Preprocessing and ROI selection, Intensity thresholding and seed selection, Multiscale segmentation and Quantitative morphological feature extraction. Experimental results show that 3dSpAn can segment individual spines from dendrites from *in vitro* and *ex vivo* samples, imaged using confocal microscopy, and *in vivo* samples, using high-resolution two-photon microscopy.

Conclusions: This freely available software will fulfill the requirement of an interactive software for quantitative morphological analysis of individual dendritic spine in 3D. The source code, windows installer, software manual and video tutorial are available at: https://sites.google.com/view/3dSpAn/.

Keywords: Dendritic spine; 3D segmentation; Interactive software; Quantitative analysis

Background

Dendritic spines are small membranous protrusions on neuronal dendrites having distinct structural features and falls in different categories based on shape and size. Generally, dendritic spine consists of spine head and thin spine neck which separates it from the parent dendrite [1] and such a specific shape helps to control electrical and biochemical compartmentalization [2]. Dendritic spines play major roles in activity and signal transmission of neural circuits, but their exact function is still not clear and under comprehensive research. The shape of dendritic spines changes spontaneously or in response to neuronal stimulation. This phenomenon is termed as structural plasticity widely considered as critical for synaptic function [3, 4]. The functional consequences of these morphological changes are not completely known yet. However, it is evident from the literature that the plasticity of dendritic spines accompany learning and memory [5] and many neuropsychiatric and neurodegenerative diseases [6, 7] e.g. Alzheimer's disease [8], schizophrenia [9]. Many aspects of the existing structure-function relationship in dendritic spines are still unknown because of their complex morphology [5, 7]. It is difficult to segment individual spine and find true spine boundaries from low resolution microscopic images which creates the challenge in accurate modeling of the three-dimensional (3D) morphology of individual spines.

With the advances in microscopic imaging technologies researchers are equipped with sufficient amount of imaging data. There is a need of robust image analysis tool to process this huge amount of imaging data for segmentation and quantitative morphological assessment of dendritic spines.

There are mainly two approaches for segmentation and morphological analysis of dendritic spines: using 2D MIP (Maximum Intensity Projection) image obtained from microscopic 3D image and directly using microcopic 3D image. The method stated in [10, 11, 12, 13] used 2D MIP image for quantitative assessment of morphological changes in dendritic spines. However, 2D MIP images are misleading due to loss of information and structure overlapping. Therefore, accurate quantitative morphological analysis of individual dendritic spine from 2-D MIP images is nearly impossible. The developed software uses 3D images for morphological analysis of dendritic spine. A few studies in the literature addressed the issue of individual spine morphometry. A commercially available tool Imaris [14] allows user for 4D analysis of den-

*Correspondence: subhadip.basu@jadavpuruniversity.in
[1]Department of CSE, Jadavpur University, 188 Raja S.C. Mullick Road, Kolkata, India
Full list of author information is available at the end of the article
†Share senior authorship

dritic spine. Imaris is good for analyzing overall spine population but it fails to assess individual spine morphometry. In [15], Swanger et al proposed a method for automatic 4D analysis of dendritc spine morphology which follows the same pipeline as Imaris. It also fails to quantify individual spine morphology. A robust user interactive tool for segmentation and morphological analysis of individual dendritic spine in 3D is still missing. In this work, we present an interactive software 3dSpAn to segment and quantitatively assess the 3D morphology of individual spines in 3D and evaluate its efficacy over different imaging conditions (*in vitro*, *ex vivo* and *in vivo*). The developed software uses 3D multiscale opening (MSO) algorithm [16] to segment the spines from the dendritic segments. The detail theoretical work and experimental results on individual spine plasticity, shown in our prior work [17], successfully validated the method with respect to the available state-of-the-art tools, like Imaris software [14] and demonstrated a high multi-user reproducibility. The objective the present work is to develop a free standalone software with user friendly GUI for segmentation and analysis of dendritic spine. Several measures have been taken to ease the user interaction process and obtain better analysis result. The challenges and our approach are discussed in detail in later sections. The detail user guide and video tutorials are available at:https://sites.google.com/view/3dSpAn/ under LGPLV3 license.

Implementation

The main advantage of 3dSpAn in comparison with other state of the art dendritic spine segmentation software is that it allows user to segment and reconstruct individual spine in 3D, extracts its quantitative morphological features and classify it into one of the three major spine classes: stubby, filopodia and mushroom.

3dSpAn is written in C++ language in Qt development environment [18]. Instead of working on the whole image, user can select different region of interest (ROI) from the image and work on them individually. 3dSpAn comprises of four main modules: Preprocessing and ROI selection(M1), Intensity thresholding and seed selection(M2), Multiscale segmentation(M3) and Quantitative morphological feature extraction(M4).

Preprocessing and ROI selection(M1)

All 3D microscopic images, irrespective of imaging modalities, have two common drawbacks: one is inherent noise and lower depth resolution than in-plane resolution. A preprocessing step is necessary to overcome these drawbacks. 3D median filter [19] is applied for noise elimination and blinear interpolation [20] is applied along the depth for appropriate scaling. Bilinear interpolation produces smooth interpolated result in real time.

After preprocessing, user selects a ROI for segmentation and quantitative morphological analyis of individual dendritic spine. Figure 1 describes the overall workflow of 3dSpAn, the different components of GUI and selected ROI. A confocal microscopic image of *in vitro* neuronal culture is used in Figure 1.

Intensity thresholding and seed selection(M2)

The benefits of working in a smaller ROI is that the intensity thresholds are better estimated and adjustment of these thresholds are also easy for a smaller ROI. For segmentation of dendritic spines, first we have to segment dendrite and spines together from the background and after that segment individual spines from the dendrite. Generally spines are of low intensity and dendrites are higher intensity but spine and dendrite share a common intensity range. Two intensity thresholds for spine and dendrite, th_s and th_d respectively are calculated for the selected ROI(R_i). Let μ be mean intensity of the ROI and δ be standard deviation then th_s and th_d are calculated as

$$th_s = \mu + \delta$$

$$th_d = \frac{I_s + 255}{2}$$

If intensity at a point $P(x, y, z)$, $I(P) < th_s$ then it is pure background point and if $I(P) \geq th_d$ then it is pure dendrite.The intensity range between th_s and th_d is the shared intensity space between spine and dendrite. A monotonically increasing fuzzy membership function is used here calculating spine and dendrite membership (μ_s and μ_d) of each pixel.

$$\mu_{spine}(P) = \begin{cases} 0, & if I(P) < th_s, \\ \frac{th_d - I_P}{th_d - th_s} & if th_s \leq I(P) < th_d, \\ 0, & if I(P) \geq th_d, \end{cases}$$

$$\mu_d(P) = \begin{cases} 0, & if I(P) \leq th_s, \\ \frac{I(P) - I_s}{th_d - th_s}, & if th_s < I(P) \leq th_d, \\ 1 & otherwise, \end{cases}$$

It may happen a spine in R_i are of high intensity($> th_d$) or a spine is disconnected from dendrite because of low intensity($< th_s$)then we have to modify the value of th_s and th_d to segment the spine. The intensity space between th_s and th_d can visualized as color transition from red to green changing from spine to dendrite. This color coded visualization helps user

to modify th_s and th_d manually. To select a dendritic spine(S_i) for segmentation user need place a spine seed on it. Multiple spine seeds can be placed for a single spine(S_i). The pixels with intensities greater than th_d are considered as implicit dendritic seeds. Explicit dendritic seeds are required if μ_d value of points are low in a dendrite region. A separator is placed to separate two touching spines. Figure 2 describes the intensity thresholding and seed selection module.

Multiscale segmentation(M3)

User given seeds and separators set stage for the MSO algorithm to segment dendrite and spine. MSO algorithm segments two conjoint objects, spines from dendrites in this case, coupled at unknown locations and arbitrary scales in the shared intensity space (bounded by th_s and th_d). With user given seeds and separators, the MSO algorithm separates the spines from the dendrites at a specific scale based on fuzzy distance transform(FDT) and fuzzy morphoconnectivity strength. After segmentation at a specific scale, the previous separation boundary is freezed using constrained morphological dilation, enabling segmentation at the next finer scale. In the iterative approach of MSO, it takes several iterations to grow path-continuity of an object starting from its seed, often falling in large-scale regions, to a peripheral location with fine scale details. Please go through Saha et. al[16] for theoretical and mathematical detail of MSO algorithm. Figure 3 describes the multiscale segmentation on the image taken in Figure 1.

Quantitative morphological feature extraction(M4)

After 3D segmentation, the feature extraction module extracts key morphological features each segmented spine S_i like volume, length, head width, and neck length from each spine. These features are extracted by identifying three characteristic points for each dendritic spine, 1) the central base point, i.e., the central point of the junction between the segmented spine and dendrite, 2) central head point, i.e., the locally deepest point in the spine, and 3) the farthest point on the spine from the central base point are determined using FDT and other morphological operations. Using these features, each S_i are categorized into one of the three major spine classes: stubby, filopodia or mushroom. Each spine shape reflects the function and strength of synaptic connections, thus the precise determination of spine morphology is crucial in studies of synaptic plasticity [21]. For the mathematical detail of the quantitative measurements and spine classification please refer to our previous paper [13]. Figure 4 describes the quantitative morphological feature extraction module.

After working on the current ROI user can select another ROI from the image and perform segmentation and analysis. It is possible to stop in between the analysis process and resume later from the saved profile.

Results and Discussion

The experiment is done on images of three different biological models *in vitro*, *ex vivo*, and *in vivo*. The details of biological models and imaging modalities are described in Table 1. For 3D visualization of the segmented spines, we used the open source software ITK SNAP [22]. The morphological feature values(volume, length, head width and neck length) of the segmented spine from confocal microscopic image of *in vitro* neuronal culture(refer Figure 4) are shown in Table 2. The performance of the software in segmentation and analysis of dendritic spine remains unchanged regardless of the biological model and imaging modality. Figure 5 and Figure 6 show the segmentation results in *ex vivo* sample and *in vivo* sample respectively. Table 3 and Table 4 show the morphological feature values of the segmented spines in Figure 5 and Figure 6. Figure 7 shows different segmented region in a a single 3D image.

Conclusions

The presented software enable user to successfully segment the dendritic spines in 3D and quantify its morphological features from images of different biological model and imaging modalities. The segmentation results are shown in *in vitro* and *ex vivo* images captured using confocal microscopy and *in vivo* image captured using two photon microscopy. The high reproducibility of segmentation method is already established in our previous publications [17, 23]. The main focus of the present work is the usability, reducing user interaction in the segmentation process and help user to estimate the segmentation parameters with enhanced visualization.

Availability and requirements

Project name: 3dSpAn
Project home page:https://sites.google.com/view/3dSpAn/
Operating system(s): Windows
Programming language: C++
License: LGPLV3
Any restrictions to use by non-academics: licence needed

List of abbreviations

MSO: Multiscale Opening, FDT: Fuzzy Distnace Transform, ROI: Region of Interest.

Availability of Data and Materials

The data used in the paper,3dSpAn windows installer,Software Manual and Video tutorial can be found at:https://sites.google.com/view/3dSpAn/

Competing interests

The authors declare that they have no competing interests.

Author's contributions

Conceived the study: S.B. and J.W. Experimental design: S.B., P.K.S., D.P., J.W. Software Development: N.D., S.B. Data Analysis: N.D., E.B., M.B., A.Z. Wrote the manuscript: S.B., N.D., E.B., J.W, E.P.

Funding

This project was supported by the Department of Biotechnology, India grant: BT/PR16356/BID/7/596/2016 (S.B) and the Polish National Science Centre, grant 2015/17/B/NZ3/00557 (J.W.). N.D. acknowledges CSIR SRF Fellowship File No. 09|096(0921)2K18 EMR-I), India. E.B. acknowledges Polish National Science Centre grant UMO-2017/27/N/NZ3/02417. DP has been supported by Polish National Science Centre (2014/15/B/ST6/05082), Foundation for Polish Science (TEAM to DP), and partially supported as RENOIR Project by the European Union Horizon 2020 research and innovation programme under the Marie Skłodowska-Curie grant agreement No 691152 and by Ministry of Science and Higher Education (Poland), grant Nos. W34/H2020/2016, 329025/PnH /2016. E.P. was supported by the Deutsche Forschungsgemeinschaft (DFG) grant PO732.

Author details

[1]Department of CSE, Jadavpur University, 188 Raja S.C. Mullick Road, Kolkata, India. [2]The Nencki Institute of Experimental Biology, Polish Academy of Sciences, Pasteura 3, 02-093, Warsaw, Poland. [3]The Institute of Physical Chemistry, Polish Academy of Sciences, Kasprzak Street 44/52, 01-224, Warsaw, Poland. [4]Centre of New Technologies, University of Warsaw, S. Banacha 2c, 02-097, Warsaw, Poland. [5]Faculty of Mathematics and Information Science, Warsaw University of Technology, Koszykowa 75, 00-662, Warsaw, Poland. [6]Department of Electrical and Computer Engineering & Department of Radiology, University of Iowa, Iowa City, IA, USA. [7]Cellular Neurophysiology, Hannover Medical School, street1 Carl-Neuberg Street, postcode30625 Hannover, Germany.

References

1. Harris, K.M., Kater, S.B.: Dendritic Spines: Cellular Specializations Imparting Both Stability and Flexibility to Synaptic Function. Annual Review of Neuroscience **17**(1), 341–371 (1994). doi:10.1146/annurev.ne.17.030194.002013
2. Lee, K.F.H., Soares, C., Béïque, J.C.: Examining form and function of dendritic spines. Hindawi Publishing Corporation (2012). doi:10.1155/2012/704103
3. Matsuzaki, M., Honkura, N., Ellis-Davies, G.C.R., Kasai, H.: Structural basis of long-term potentiation in single dendritic spines. Nature **429**(6993), 761–766 (2004). doi:10.1038/nature02617
4. Caroni, P., Donato, F., Muller, D.: Structural plasticity upon learning: regulation and functions. Nature Reviews Neuroscience **13**(7), 478–490 (2012). doi:10.1038/nrn3258
5. Sala, C., Segal, M.: Dendritic Spines: The Locus of Structural and Functional Plasticity. Physiological Reviews **94**(1), 141–188 (2014). doi:10.1152/physrev.00012.2013
6. Fiala, J.C., Spacek, J., Harris, K.M.: Dendritic spine pathology: Cause or consequence of neurological disorders? Brain Research Reviews **39**(1), 29–54 (2002). doi:10.1016/S0165-0173(02)00158-3
7. Chidambaram, S.B., Rathipriya, A.G., Bolla, S.R., Bhat, A., Ray, B., Mahalakshmi, A.M., Manivasagam, T., Thenmozhi, A.J., Essa, M.M., Guillemin, G.J., Chandra, R., Sakharkar, M.K.: Dendritic spines: Revisiting the physiological role. Progress in Neuro-Psychopharmacology and Biological Psychiatry **92**, 161–193 (2019). doi:10.1016/j.pnpbp.2019.01.005
8. Spires, T.L., Meyer-Luehmann, M., Stern, E.A., McLean, P.J., Skoch, J., Nguyen, P.T., Bacskai, B.J., Hyman, B.T.: Dendritic spine abnormalities in amyloid precursor protein transgenic mice demonstrated by gene transfer and intravital multiphoton microscopy. Journal of Neuroscience **25**(31), 7278–7287 (2005). doi:10.1523/JNEUROSCI.1879-05.2005
9. Glausier, J.R., Lewis, D.A.: Dendritic spine pathology in schizophrenia. Neuroscience **251**, 90–107 (2013). doi:10.1016/j.neuroscience.2012.04.044
10. Wong, S.T.C., Chen, X., Xu, X.: Methods and systems for the analysis of 3d microscopic neuron images (2006). http://www.google.com.gt/patents/WO2006125188A1?cl=en
11. Ruszczycki, B., Wlodarczyk, J., Kaczmarek, L.: Method and a system for processing an image comprising dendritic spines. Google Patents (2012)
12. Ruszczycki, B., Szepesi, Z., Wilczynski, G.M., Bijata, M., Kalita, K., Kaczmarek, L., Wlodarczyk, J.: Sampling issues in quantitative analysis of dendritic spines morphology. BMC Bioinformatics **13**(1), 213 (2012). doi:10.1186/1471-2105-13-213
13. Basu, S., Plewczynski, D., Saha, S., Roszkowska, M., Magnowska, M., Baczynska, E., Wlodarczyk, J.: 2dSpAn: semiautomated 2-d segmentation, classification and analysis of hippocampal dendritic spine plasticity. Bioinformatics **32**(16), 2490–2498 (2016). doi:10.1093/bioinformatics/btw172
14. Worbs, T., Förster, R.: 4D-Tracking with Imaris (2007). http://www.bitplane.com/learning/4d-tracking-with-imaris-immunology Accessed 2018-01-17
15. Swanger, S.A., Yao, X., Gross, C., Bassell, G.J.: Automated 4D analysis of dendritic spine morphology: applications to stimulus-induced spine remodeling and pharmacological rescue in a disease model. Molecular Brain **4**(1), 38 (2011). doi:10.1186/1756-6606-4-38
16. Saha, P.K., Basu, S., Hoffman, E.A.: Multiscale Opening of Conjoined Fuzzy Objects: Theory and Applications. IEEE Transactions on Fuzzy Systems **24**(5), 1121–1133 (2016)
17. Basu, S., Saha, P.K., Roszkowska, M., Magnowska, M., Baczynska, E., Das, N., Plewczynski, D., Wlodarczyk, J.: Quantitative 3-D morphometric analysis of individual dendritic spines. Scientific Reports **8**(1), 3545 (2018). doi:10.1038/s41598-018-21753-8
18. Qt Cross-platform software development for embedded and desktop. https://www.qt.io/ Accessed 2019-11-05
19. Brownrigg, D.R.K.: The Weighted Median Filter. Communications of the ACM **27**(8), 807–818 (1984). doi:10.1145/358198.358222
20. Gribbon, K.T., Bailey, D.G.: A novel approach to real-time bilinear interpolation. In: Proceedings, DELTA 2004 - Second IEEE International Workshop on Electronic Design, Test and Applications, pp. 126–131 (2004). doi:10.1109/DELTA.2004.10055
21. Kasai, H., Matsuzaki, M., Noguchi, J., Yasumatsu, N., Nakahara, H.: Structure–stability–function relationships of dendritic spines. Trends in Neurosciences **26**(7), 360–368 (2003). doi:10.1016/S0166-2236(03)00162-0
22. Yushkevich, P.A., Piven, J., Hazlett, H.C., Smith, R.G., Ho, S., Gee, J.C., Gerig, G.: User-guided 3D active contour segmentation of anatomical structures: significantly improved efficiency and reliability. Neuroimage **31**(3), 1116–1128 (2006)
23. Krzystyniak, A., Baczynska, E., Magnowska, M., Antoniuk, S., Roszkowska, M., Zareba-Koziol, M., Das, N., Basu, S., Pikula, M., Wlodarczyk, J.: Prophylactic Ketamine Treatment Promotes Resilience to Chronic Stress and Accelerates Recovery: Correlation with Changes in Synaptic Plasticity in the CA3 Subregion of the Hippocampus. International Journal of Molecular Sciences **20**(7), 1726 (2019). doi:10.3390/ijms20071726
24. Magnowska, M., Gorkiewicz, T., Suska, A., Wawrzyniak, M., Rutkowska-Wlodarczyk, I., Kaczmarek, L., Wlodarczyk, J.: Transient ecm protease activity promotes synaptic plasticity. Scientific reports **6**, 27757 (2016)
25. Szepesi, Z., Bijata, M., Ruszczycki, B., Kaczmarek, L., Wlodarczyk, J.: Matrix metalloproteinases regulate the formation of dendritic spine head protrusions during chemically induced long-term potentiation. PLoS One **8**(5), 63314 (2013)
26. Kim, B.G., Dai, H.-N., McAtee, M., Vicini, S., Bregman, B.S.: Labeling of dendritic spines with the carbocyanine dye dii for confocal microscopic imaging in lightly fixed cortical slices. Journal of neuroscience methods **162**(1-2), 237–243 (2007)
27. Łukasiewicz, K., Robacha, M., Bożycki, Ł., Radwanska, K.,

Czajkowski, R.: Simultaneous two-photon in vivo imaging of synaptic inputs and postsynaptic targets in the mouse retrosplenial cortex. JoVE (Journal of Visualized Experiments) (109), 53528 (2016)
28. Trachtenberg, J.T., Chen, B.E., Knott, G.W., Feng, G., Sanes, J.R., Welker, E., Svoboda, K.: Long-term in vivo imaging of experience-dependent synaptic plasticity in adult cortex. Nature **420**(6917), 788 (2002)
29. Holtmaat, A., de Paola, V., Wilbrecht, L., Trachtenberg, J.T., Svoboda, K., Portera-Cailliau, C.: Imaging neocortical neurons through a chronic cranial window. Cold Spring Harbor Protocols **2012**(6), 069617 (2012)
30. Chow, D.K., Groszer, M., Pribadi, M., Machniki, M., Carmichael, S.T., Liu, X., Trachtenberg, J.T.: Laminar and compartmental regulation of dendritic growth in mature cortex. Nature neuroscience **12**(2), 116 (2009)

Figures

Figures

Tables

Additional Files

Additional file 1 — Sample additional file title
Additional file descriptions text (including details of how to view the file, if it is in a non-standard format or the file extension). This might refer to a multi-page table or a figure.

Additional file 2 — Sample additional file title
Additional file descriptions text.

Table 1 Details of different imaging protocols.

	In-vitro	***Ex-vivo***	***In-vivo***
Methodological approach	primary neuronal culture/dissociated neuronal culture	brain slices	living animal
Animal	rat	mice	mice
Dendritic spine visualization method	transfection with EGFP plasmid under the control of synapsin-1 promoter at 14 day in vitro (DIV) of hippocampal neurons	DiI staining on fixed tissue	2-photon imaging by cranial windows of transgenic mouse line (Thy1-GFP) expressing GFP under the thy1 promoter allowing visualization of the neurons in prefrontal cortex
	GFP fluorescence	DiI fluorescence (red fluorescence channel)	GFP/YFP fluorescence
Protocols used in: [13, 17]	**Primary hippocampal cultures from** $P0$ (post-natal Day 0) Wistar rats were prepared as described later. Brains were removed and hippocampi were isolated on ice in dissociation medium DM; $81.8mM$ Na2SO4, $30mM$ K2SO4, $5.8mM$ MgCl2, $0.25mM$ CaCl2, $1mM$ HEPES pH 7.4, $20mM$ glucose; $1mM$ kynureic acid; 0.001% Phenol Red. Next, hippocampi were incubated twice for $15min$ at $37°C$ with 100 units of papain (Worthington, NY) in DM, then rinsed three times in DM and subsequently three times in plating medium [MEM, 10% fetal bovine serum and 1% penicilin-streptomycin]. Hippocampi were triturated in plating medium, then centrifuged for $10min$ at room temperature, at $208.5g$. The resulting cell pellet was suspended in plating medium, cells were counted and plated at density 120000 cells per $18mm$ diameter coverslip (Assistent, Germany) coated with $1mg/ml$ poly-L-lysine (Sigma) and $2.5\mu g/ml$ laminin (Roche). At $3h$ after plating medium was exchanged for maintenance medium (Neurobasal-A without Phenol Red, 2% B-27 supplement, 1% penicillin-streptomycin, $0.5mM$ glutamine, $12.5\mu M$ glutamate, $25\mu M$ β-mercaptoethanol) and cells were kept at $37°C$ under a humidified 5% $CO2$ atmosphere.	**DiI staining** was performed in brain slices from $C57BL6J$ mice. The mice were anesthetized and transcardially perfused with 1.5% paraformaldehyde. The brains were dissected and sliced using a vibratome. Slices ($140\mu m$ thick) were allowed to recover for at least $1.5h$ at room temperature. Random dendrite labeling was performed using $1.6mm$ tungsten particles (Bio-Rad, Hercules, CA, USA) that were coated with propelled lipophilic fluorescent dye($1,1'$-dioctadecyl-$3,3,3,3'$-tetramethylindocarbocyanine perchlorate), (DiI; Invitrogen) that was delivered to the cells by gene gun (Bio-Rad) bombardment.	**Virus injections** Implant cranial windows and inject HAPLN1-Scarlet + Synaptophysin-BFP AAVs in PFC for Thy1-GFP mice. Imaging after 4 weeks postinjection: Anaesthetize with Isoflurane to perform baseline images (3 to 4 positions) and $24hours$ after performance of single image for all positions.
Imaging protocols	**Live cell imaging** Cultured hippocampal neurons were transfected at $14days$ *In-vitro* (DIV) with Syn-GFP plasmid to visualize neuronal morphology. Live cell imaging was performed on $20\breve{}22$ DIV. Prior the imaging, the cells were placed in an acquisition chamber with controlled temperature ($37°C$) and stable CO2 5% concentration. Dendritic segments decorated with dendritic spines were imaged at the Time 0, before stimulation, and then was induced by bath application of a mixture of $50\mu M$ forskolin, $50\mu M$ picrotoxin and $0.1\mu M$ rolipram (each dissolved in DMSO) in maintenance media. Dendritic segments were imaged at $10min$ after cLTP induction. Images were acquired using the Carl Zeiss LSM780 confocal microscope with a C-Apochromat 40x/1.2 NA water immersion objective using $488nm$ wavelength argon laser at 3% transmission at $70nm/pixel$ resolution. A series of z-stacks were acquired at $0.4\mu m$ step.	**Imaging** Images of dendrites in different brain regions were acquired under 561 nm fluorescent illumination using a confocal microscope ($63'$ objective, 1.4 NA) at a pixel resolution of 1024×1024 with a 3.43 zoom, resulting in a $0.07\mu m$ pixel size [24].	**Imaging** Images of dendrites in different brain regions were acquired under $488nm$ fluores-cent illumination using a 2-photon microscope ($40'$objective) with a 2.0 zoom.
Procedure references	Refer [24, 25]	Refer [24, 26]	Refer [27, 28, 29, 30]
Aparatus	Fluorescent confocal microscopy equipped with live cell imaging setup (Zeiss LSM780)	Fluorescent confocal microscopy (Zeiss LSM800)	2-photon microscopy (Zeiss LSM 7 MP Axio Examiner.Z1)

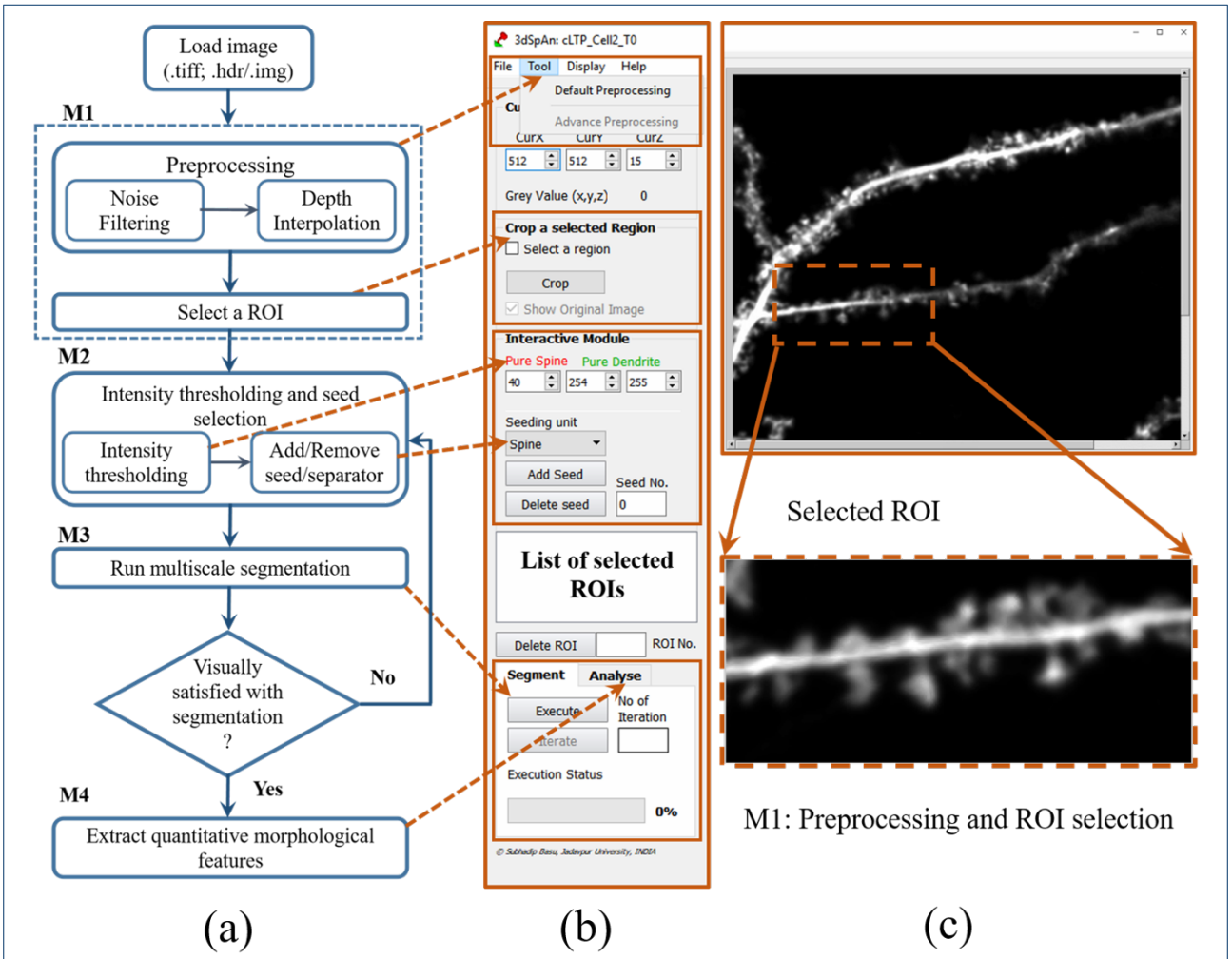

Figure 1 Brief representation of the 3dSpAn workflow, the GUI and the module M1. (a) Workflow diagram of 3dSpAn.The blocks are representing four main modules: M1, M2, M3 and M4 (b)Shows the working panel of the GUI. The main modules are enclosed with rectangular boxes and arrow connected to the appropriate blocks of the workflow diagram to describe its functionality. (c) An image of *In vitro* neuronal culture is loaded in GUI (above) and a ROI is selected (shown in dotted rectangular box) with the help of the GUI. The zoomed version of selected ROI is shown below the full image.

Table 2 Morphological features like, volume, length, head width, neck length, and type of dendritic spines are extracted from each spine shown in Figure 4(a).

Spine ID	Volume ($micron^3$)	Length ($micron$)	Head Width ($micron$)	Neck Length ($micron$)	Type
1	0.197762	0.759	0.4278	0.069	Filopodia
2	0.491449	0.3312	0.6624	0	Stubby
3	1.439855	0.5313	1.0212	0	Stubby
4	2.241417	1.725	1.173	0.207	Mushroom
5	1.418173	1.311	1.1454	0.207	Mushroom
6	0.383041	0.2898	0.5796	0	Stubby
7	0.568649	0.276	0.552	0	Stubby
8	1.484204	0.5796	0.966	0	Stubby
9	0.499005	0.3795	0.759	0	Stubby
10	0.94742	0.4002	0.8004	0	Stubby
11	0.473381	0.3312	0.6624	0	Stubby
12	0.422463	0.276	0.552	0	Stubby
13	1.060755	0.5244	0.8004	0	Stubby
14	1.025934	1.035	0.9246	0.138	Mushroom
15	1.607723	0.5796	1.1316	0	Stubby
16	0.425748	0.3588	0.552	0	Stubby
17	0.304199	0.2898	0.5244	0	Stubby

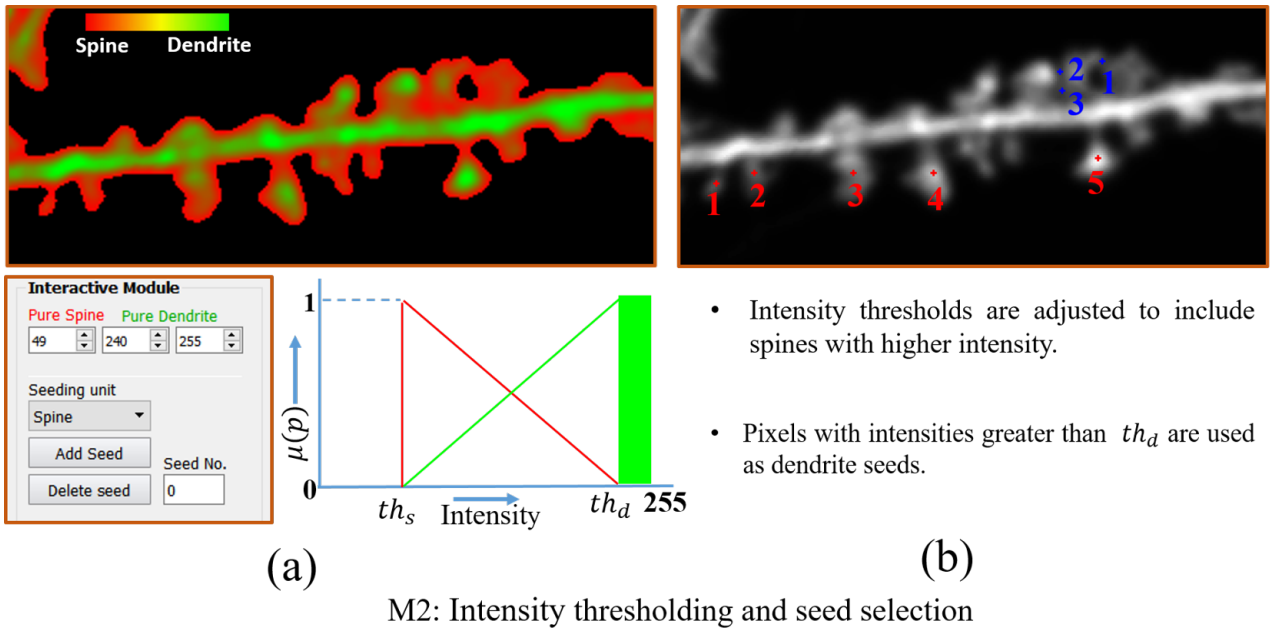

Figure 2 Representation of the M2 module. (a) Visualization of the shared intesity space between spine and dendrite on the selected ROI of Figure 1(c) with color transition from red to green describing the spine membership and dendrite membership value of a pixels(above). The block interactive module show the intensity thresholds th_s(40) and th_d(240) for the spine and dendrite respectively and the graph shows fuzzy membership curve for both spine(red) and dendrite(green). (b) Some of the user given spine seeds (red) and separators(blue) which are place on the same depth are shown. The seeds are numbered in the order they are given. Often, to include a spine user need to adjust th_s and th_d. The pixels with greater than th_d are used as dendrite seeds implicitly. For this ROI, explicit dendrite seeds are not given.

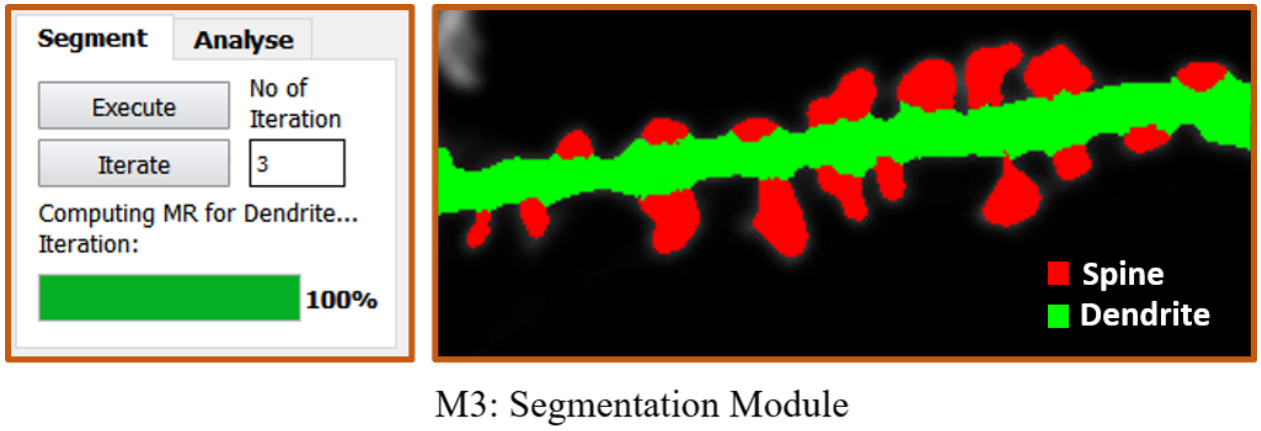

Figure 3 Shows M3 module and the segmented spine from the selected ROI of Figure 1(c). The segmentation module of the GUI shows the number of times the MSO algorithm iterate to achieve the segmentation result.

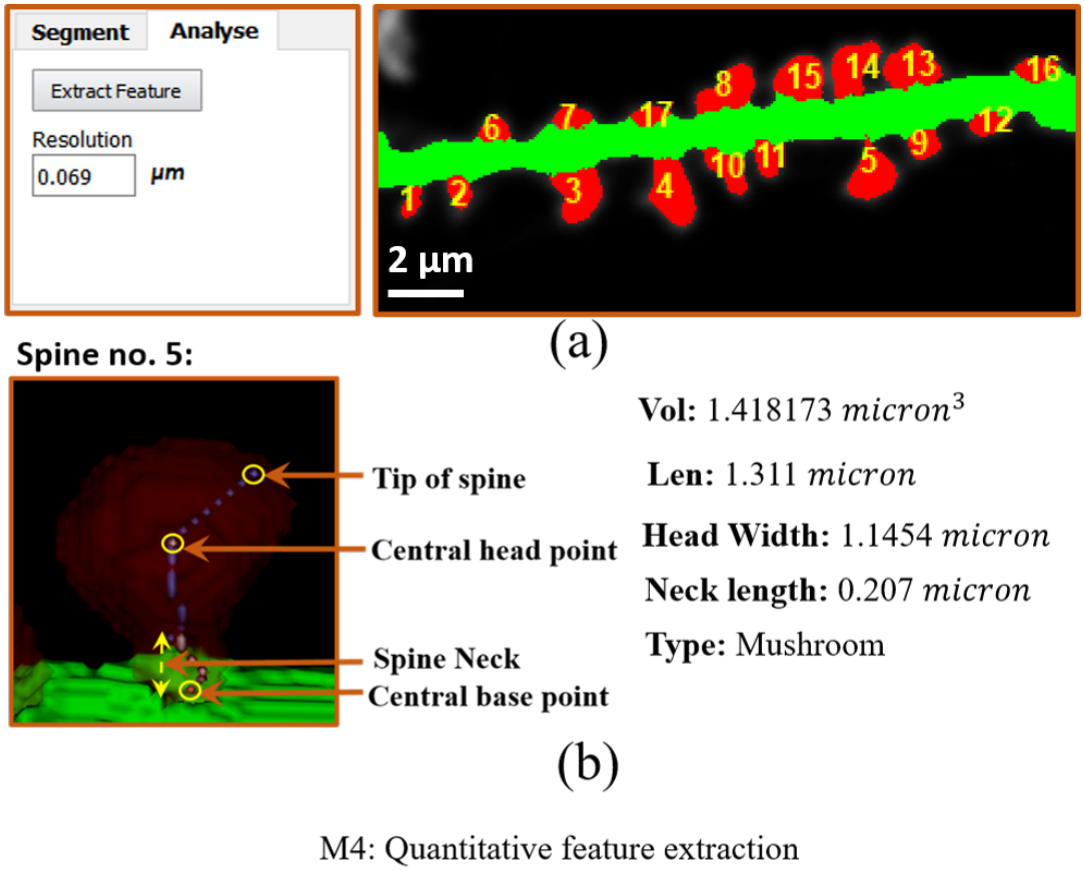

Figure 4 Description of module M4. (a) After quantitative morphological feature extraction, the spine are numbered in the order same as user given spine seeds. (b) Zoomed and rotated 3D view of spine no. 5. The spine is visualized in popular ITK-Snap software [22]. The transparent visualization helps to see the calculated path and points inside spine. Key points like Central base point, Central head point and Tip of the spine are marked (small yellow circle) and calculated for measurement of spine volume, spine length, head width, neck and length. Based on these measurements, spine classification is done. Here the spine belongs to Mushroom class.

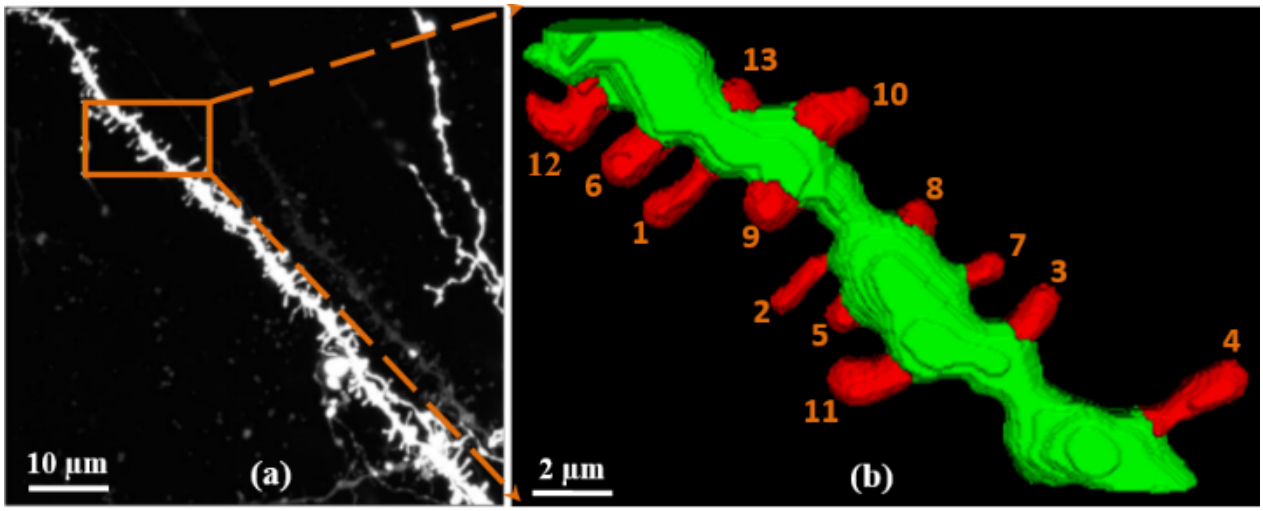

Figure 5 3D reconstruction and morphological feature extraction of the segmented dendritic spines obtained from *ex vivo* model of mouse brain slices with selected rectangular region (a), 3D reconstruction of the dendritic segmentation with individual spine numbering (b).

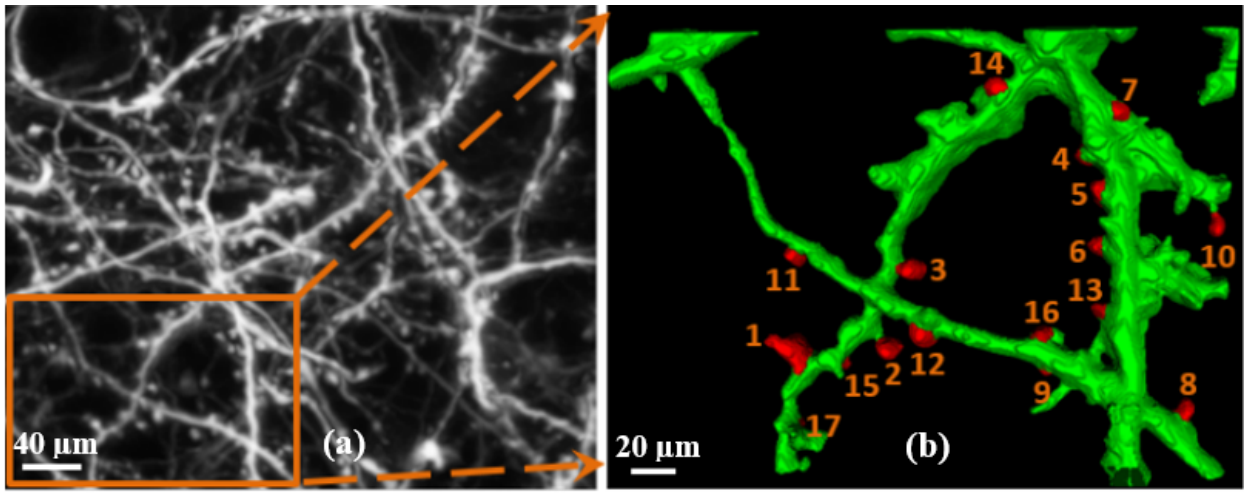

Figure 6 3D reconstruction and morphological feature extraction of the segmented dendritic spines obtained from *in vivo* two-photon imaging with selected rectangular region (a), 3D reconstruction of the dendritic segmentation with individual spine numbering (b) .

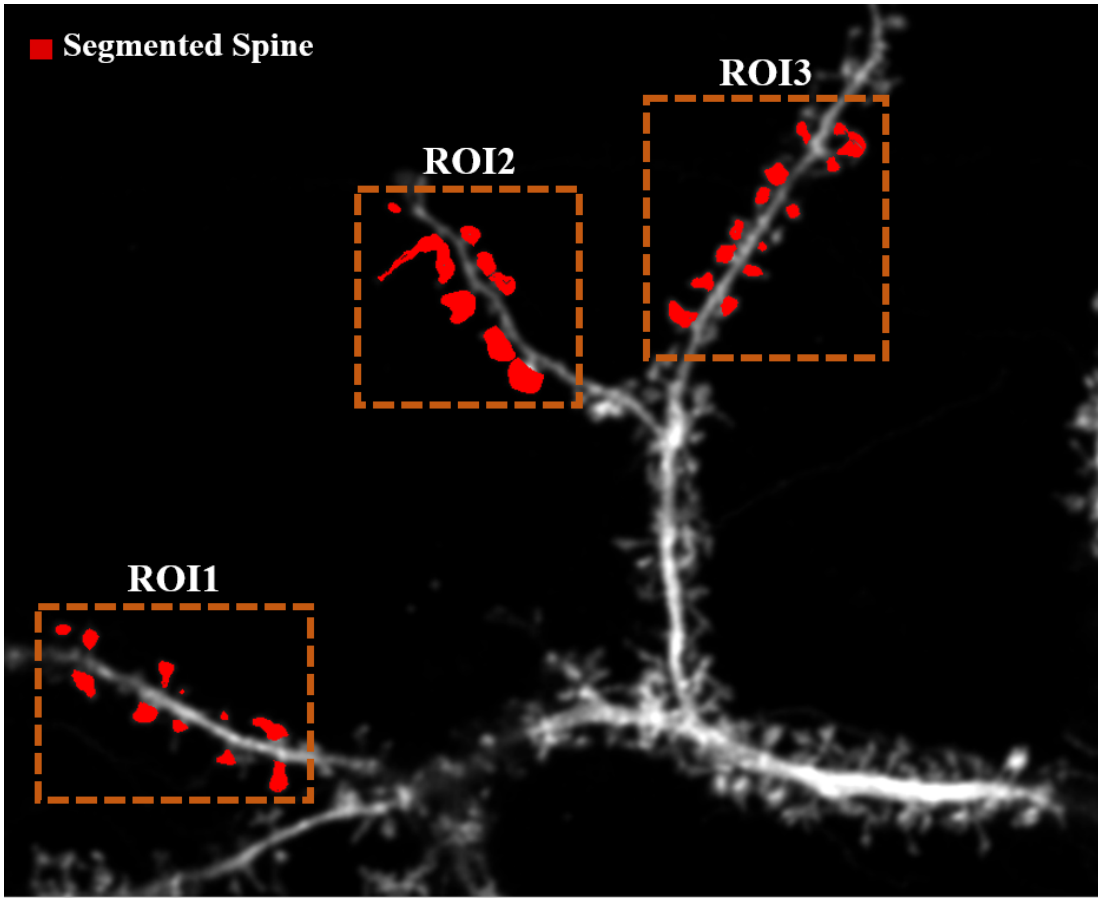

Figure 7 Different segmented regions (ROI1, ROI2 and ROI3, enclosed in dotted rectangular box) in a confocal light microscopic image of *In-vitro* neuronal culture. Segmented spines are shown in red color.

Table 3 Morphological features like, volume, length, head width, neck length and type of dendritic spines are extracted from each spine shown in Figure 5.

Spine ID	Volume ($micron^3$)	Length ($micron$)	Head Width ($micron$)	Neck Length ($micron$)	Type
1	0.847225	1.38	0.8556	0.552	Mushroom
2	0.364316	1.104	0.5244	0.276	Filopodia
3	0.728961	0.5244	0.8556	0	Stubby
4	1.395506	2.208	0.966	0.966	Mushroom
5	0.322924	0.4209	0.7038	0	Stubby
6	1.138612	0.8418	1.035	0	Stubby
7	0.309127	0.4692	0.621	0	Stubby
8	0.447429	0.4071	0.69	0	Stubby
9	0.950048	0.5796	1.0764	0	Stubby
10	0.983227	0.5037	0.9384	0	Stubby
11	1.569944	1.518	1.0212	0.207	Mushroom
12	1.379409	3.864	0.4692	0.483	Filopodia
13	0.386984	0.3519	0.7038	0	Stubby

Table 4 Morphological features like, volume, length, head width, neck length and type of dendritic spines are extracted from each spine shown in Figure 6.

Spine ID	Volume ($micron^3$)	Length ($micron$)	Head Width ($micron$)	Neck Length ($micron$)	Type
1	1.120873	1.242	0.966	0.069	Mushroom
2	0.329823	0.897	0.6624	0.138	Mushroom
3	0.483565	1.035	0.6486	0.138	Mushroom
4	1.917178	1.311	0.621	0.414	Mushroom
5	0.732575	0.345	0.6624	0	Stubby
6	0.519373	0.4071	0.8142	0	Stubby
7	0.375157	0.3795	0.6624	0	Stubby
8	0.64552	0.4485	0.621	0	Stubby
9	0.38567	0.345	0.6624	0	Stubby
10	0.506232	1.242	0.69	0.621	Mushroom
11	0.509517	0.759	0.4692	0.069	Mushroom
12	1.406018	0.345	0.69	0	Stubby
13	0.370887	0.0966	0.1932	0	Stubby
14	0.318654	0.1656	0.3312	0	Stubby
15	0.289745	0.2829	0.552	0	Stubby
16	0.490464	0.1932	0.3864	0	Stubby
17	0.122534	0.1932	0.3312	0	Stubby